Influence of the Meridional Shifts of the Kuroshio and the Oyashio Extensions on the Atmospheric Circulation

Claude Frankignoul and Nathalie Sennéchael

LOCEAN / IPSL, Université Pierre et Marie Curie Paris, France

Young-Oh Kwon

Woods Hole Oceanographic Institution, Woods Hole, Massachusetts, USA

Michael A. Alexander

NOAA/ESRL, Boulder, CO

Submitted to Journal of Climate

Corresponding author: cf@locean-ipsl.upmc.fr

Abstract

The meridional shifts of the Oyashio Extension (OE) and of the Kuroshio Extension (KE), as derived from high-resolution monthly sea surface temperature (SST) anomalies in 1982-2008 and historical temperature profiles in 1979-2007, respectively, are shown based on regression analysis to significantly influence the large-scale atmospheric circulation. The signals are independent from the ENSO teleconnections, which were removed by seasonally varying, asymmetric regression onto the first three principal components of the tropical Pacific SST anomalies. The response to the meridional shifts of the OE front is equivalent barotropic and broadly resembles the North Pacific Oscillation / Western Pacific pattern in a positive phase for a northward frontal displacement. The response reaches 35 m at 250 hPa for a typical OE shift, a strong sensitivity since the associated SST anomaly is 0.5 K. However, the amplitude depends on an assumed 2-month atmospheric response time. The response is stronger during winter and when the front is displaced southward. The response to the northward KE shifts primarily consists of a high centered in the northwestern North Pacific and hemispheric teleconnections. It is also equivalent barotropic, except near Kamchatka where it tilts slightly westward with height. The typical amplitude is half as large as that associated with OE shifts. Dynamical feedbacks are suggested by the wind stress curl response to the two western boundary currents.

1. Introduction

Observational evidence that extratropical sea surface temperature (SST) anomalies have an influence on the large-scale atmospheric circulation during certain seasons has been found in the North Atlantic (Czaja and Frankignoul 1999, 2002; Rodwell and Folland 2002) and the North Pacific (Liu et al. 2006; Frankignoul and Sennéchael 2007; Qiu et al. 2007). These air-sea interactions are highly relevant to the short-term climate predictability, as the SST anomalies tend to be rather persistent because of SST anomaly reemergence, sustained forcing from the tropics, and low-frequency changes in oceanic heat advection. The extratropical SST variability is large near the strong SST gradients along the oceanic fronts associated with western boundary currents and their extensions (hereafter WBCs), especially at decadal time scales (e.g., Nakamura et al. 1997; Nakamura and Kasmin 2003; Kwon et al. 2010a), when the changes in the oceanic circulation are particularly effective in affecting the SST (e.g., Qiu 2002; Vivier et al. 2002; Schneider et al. 2002).

Major storm tracks are organized along or just downstream of the main oceanic frontal zones. Nakamura et al. (2004) argued that differential heat supply across a midlatitude frontal zone acts to maintain surface baroclinicity, sustaining storm development and the anchoring effect of the SST frontal zones, as found by Taguchi et al. (2009) for the Kuroshio and Oyashio Extension (KOE) region during spring. In the mean, the large heat release from the Gulf Stream forces a basin-scale tropospheric response (Minobe et al. 2008), but the large-scale influence of anomalous frontal displacement remains to be established.

As reviewed by Small et al. (2008), there is ample evidence that the atmospheric boundary layer is locally affected by the SST variability near oceanic fronts. Although observational attempts to relate large-scale tropospheric fluctuations in the North Atlantic sector to prior changes of the Gulf Stream have failed (Frankignoul et al. 2001), there is

growing observational evidence that an active air-sea coupling involving oceanic circulation changes may be at play in the North Pacific. Liu et al. (2006) showed that the summer atmospheric circulation was linked to SST changes in the preceding winter. Frankignoul and Sennéchael (2007, hereafter FS07) found that a primarily equivalent barotropic atmospheric signal in late summer was significantly correlated with previous SST anomalies with a large center of action in the Kuroshio Extension (KE). The SST anomaly pattern was basin-wide, however, with the KE anomaly surrounded by anomalies of the opposite polarity, resembling, although shifted slightly south, the Pacific Decadal Oscillation (PDO, Mantua et al. 1997), so that the atmospheric response could not solely be attributed to changes in the KE region. Qiu et al. (2007) found a relation between winter KE SST anomalies and wind stress curl in the following spring, which was noisy but showed a zonal dipolar structure that could lead to a weak delayed negative feedback on the KE variability and enhance its decadal variability. However, lacking a reliable indicator of the KE jet changes, these signals could not be firmly linked to the oceanic circulation.

More direct evidence of WBC influence on the atmospheric circulation was recently provided by Hirose et al. (2009), who showed that changes in the Tsushima Warm Current (a current fed by the Kuroshio which passes between Korea and Japan) during autumn were robustly correlated with the Western Pacific (WP) pattern and its surface counterpart - the North Pacific Oscillation (NPO), the second dominant mode of wintertime sea level (SLP) variability in the North Pacific (e.g., Wallace and Gutzler 1981; Linkin and Nigam 2008), during the following winter. Joyce et al. (2009) found that the large-scale shifts in the Gulf Stream and the KE path were causing significant changes in the year-to-year near-surface synoptic activity.

There are two frontal zones in the western North Pacific, the subtropical front associated with the KE and the subarctic front associated with the Oyashio Extension (hereafter OE). The KE front is deep but has a modest SST gradient while the OE is shallow and has a strong SST gradient, and their decadal variability is not necessarily coherent (Nonaka et al. 2006). Previous studies have shown that the KE responds to basin-scale wind forcing with a delay of 2 to 4 years linked to baroclinic Rossby wave propagation (e.g. Seager et al. 2001; Schneider et al. 2002; Qiu 2003). Based on satellite altimetry data, Qiu and Chen (2005) found that the KE path tends to migrate northward when the KE jet strengthens, and vice versa. On the other hand, Taguchi et al. (2007) suggested based on an eddy-resolving oceanic hindcast that this variability can be separated into two leading EOFs of KE SSH. The first EOF mostly describes the meridional shifts of the KE, which are linked to the Aleutian Low and the PDO, and the second describes changes in the KE strength, which are mainly linked to the North Pacific Gyre Oscillation and forced by the NPO (Ceballos et al. 2009). However, the two modes are not well separated in the satellite altimetry era nor in the period considered in this paper, and EOFs artificially separate a shift and intensification into two independent modes (Qiu and Chen 2010). The transport of the Oyashio rapidly responds to the wind stress changes associated with the Aleutian low and associated Pacific-North American (PNA) pattern via barotropic Rossby wave propagation (e.g. Isoguchi et al. 1997), and to local Ekman pumping via baroclinic wave propagation. It is also remotely forced near 160°-170°E about 3 yr before (Qiu 2002; Nonaka et al. 2008).

If the WBC influence on the large-scale atmospheric circulation reinforces or damps the atmospheric modes that mainly force the WBC changes (i.e. two-way coupling), it could enhance the decadal climate variability. Several climate model simulations suggest that this occurs in the North Pacific (e.g., Latif and Barnet 1994; Pierce et al. 2001; Kwon and Deser

2007). The dominant mechanisms involve basin-scale wind stress curl forcing associated with, for example, a deepening of the Aleutian low, Rossby wave propagation and spin-up of the subtropical gyre, which increases SST in the KOE. The negative surface heat flux feedback then leads to an atmospheric response that initiates the opposite phase of the oscillation, resulting in a stochastically forced system with delayed negative feedback. However, the large-scale atmospheric response differs among the modeling studies, and the horizontal resolution is insufficient to resolve the dual fronts in the western North Pacific.

The extratropical atmospheric circulation and SST anomalies in the North Pacific are strongly influenced by the El Niño-Southern Oscillation phenomenon (ENSO). The ENSO teleconnections substantially contribute to the forcing of main modes of climate variability such as the PDO, and they affect the oceanic circulation (e.g., Alexander et al. 2002; Schneider and Cornuelle 2005). Although the climatic impact and predictability of the teleconnections is of much interest, they make it difficult to separate the atmospheric response to extratropical boundary forcing. Indeed, the main assumption in empirically estimating the atmospheric response to extratropical SST anomalies is that the time scale of the latter is much larger than that of the atmosphere. If the assumption is valid, the atmospheric response can be derived from the relation between prior SST anomalies and the atmosphere (Frankignoul et al. 1998), but this assumption does not hold in the presence of substantial ENSO teleconnections, which have a time scale comparable to that of the extratropical SST anomalies. Previous observational studies of North Pacific SST influence have attempted to remove the ENSO signal by regression, using various degrees of complexity ranging from linear regression on the concurrent NINO 3.4 index (Qiu et al. 2007), regression on the time lagged NINO 3.4 index (Liu et al. 2006), to seasonally varying regression on two ENSO indices (Frankignoul and Kestenare 2002, FS07). The amount of removed variance from the

monthly SST and the atmospheric anomaly fields was substantial in certain areas (as much as 35% for SST north of 20°N and 25% for the geopotential height in FS07), but there has been no attempt to compare the removed signal to more usual ENSO estimates, such as based on composites. This will be done here, allowing for a better estimate of the success of the filtering process.

Section 2 describes the observational data used in this study. Section 3 describes how the WBC indices are constructed and briefly discusses their relation to SST and previous atmospheric forcing. Section 4 gives the methodology used to determine the WBC influence on the atmosphere and remove the ENSO influence. The atmospheric response to the OE and KE shifts is investigated in Section 5. Conclusions are given in Section 6.

2. Data

Monthly anomalies of SLP, geopotential height at 250 and 500 hPa (hereafter Z250 and Z500), surface wind stress, and SST were taken from the NCEP-NCAR reanalysis (Kistler et al. 2001) for the period 1980 – 2008. We also considered version 2 of the NOAA Optimal Interpolation ¼° daily SST (AVHRR-only product) (NOAA OI SST, Reynolds et al. 2007) for the period 1982 – 2008. The North Pacific SST climatology and the standard deviation of the monthly SST anomalies are shown in Fig. 1a. The SST variability is largest in the KOE region, peaking near the OE front. However, the NCEP-NCAR reanalysis uses the coarse resolution SST, so that the atmospheric circulation does not respond to small-scale SST variations. Yet, it is expected that the atmospheric observations assimilated in the model nudge the large-scale response to the SSTs to the one driven by the small shifts in the KOE fronts. The bottom panel in Fig. 1 shows the time evolution of the SST anomaly in a box centered on the KE (30°-40°N, 143°E-183°W) that was shown in FS07 to be representative of

the oceanic forcing of the atmosphere in summer, and also corresponds to the largest variability at depth. The time series exhibits an upward trend, large decadal variability and a high negative correlation (r = -0.72) with the PDO index.

Additionally, the raw temperature profiles for 1979-2007 from the World Ocean Database 2005 (Johnson et al. 2006, available at http://www.nodc.noaa.gov/OC5/WOD05/docwod05.html, and its online update (http://www.nodc.noaa.gov/OC5/WOD05/pr_wod05.html) were used to objectively map 200 m temperature and calculate the KE index.

3. **Variability of the Kuroshio and Oyashio Extensions, and their links to SST**

a. Definition of the OE index

The OE index (OEI) is defined as the leading principal component (PC) of the latitude of the maximum meridional SST gradient (dSST/dy) between 145° and 170°E. Longitudes west of 145°E were excluded because the OE is not clearly distinct from the KE there, and longitudes east of 170°E were not considered because the OE front becomes too diffuse. First, dSST/dy was calculated from the monthly mean NOAA OI SST with 0.25° resolution for 1982-2008. Then, the latitude of OE at each longitude and month was taken as the latitude of maximum dSST/dy between 35°N and 47°N (Fig. 2a). After removing a linear trend and the mean seasonal cycle at each longitude, EOFs were calculated for the monthly OE latitude. The leading EOF represents a coherent north-south shift explaining 13% of the total variance (Fig. 2b). A similar EOF pattern, but with 32% of the total variance explained, is obtained when a moving average with a 13-month triangular weight is applied before the EOF calculation. However, the unsmoothed OE index (Fig. 3b) will be used since it provides

higher temporal resolution, which is more appropriate to detect an atmospheric response that involves a response time of a couple of months.

After removal of a third-order trend, the regression of SLP on the OEI when SLP leads by 0-2 yr yields atmospheric forcing patterns that resemble the Aleutian Low mode, as illustrated in Fig. 4. A weaker Aleutian Low (positive SLP anomalies) drives a northward shift of the OE, consistent with the modeling study by Nonaka et al. (2008). However, at most lags the SLP anomaly has its center of action between 40° and 50°N, which is slightly south of that of the typical Aleutian Low mode, and it often has a weaker high over the Bering Sea. The wind stress curl forcing patterns exhibit zonally elongated negative anomalies between 35° and 50°N, consistent with the resulting northerly OE location. At short lags, the maximum wind stress curl is in the central basin, while it is to the west of the dateline when the wind stress curl leads by 2 yr. Nonaka et al. (2008) attributed the fast response to basin-wide wind stress curl anomalies and barotropic Rossby wave adjustment, and the slow (~3year) response to wind stress curl anomalies confined to the east of 170°E and baroclinic Rossby wave adjustment. We used a linear baroclinic Rossby wave model forced by the monthly wind stress curl anomalies to simulate the slow baroclinic OE response (and KE changes in the next section) as in Qiu (2003). The correlation between the sea surface height (SSH) hindcast (averaged over 38-45°N, 145-170°E) and the OEI peaks when the OEI leads by 1-2 yr ($r = 0.32$ with monthly resolution and $r = 0.59$ with annual resolution), consistent with the slow baroclinic OE response.

The associated SST pattern based on the smoother NCEP-NCAR product[1] is shown in Fig. 5. As expected, the SST anomaly is large and positive when the OE front is in a northerly position (positive OEI), but it is much broader than expected from the front displacement

[1] Similar, but more noisy, results are found with the high-resolution SST data

alone. It is basin-wide, primarily reflecting the Ekman transport associated with the atmospheric fluctuations that displaced the front. Nonaka et al. (2008) also reported a positive correlation between the OE latitude and the SST anomalies in their eddy-resolving ocean model simulation. The OEI is significantly correlated with the KE SST index and the PDO (Fig. 1) at zero lag (respectively r = 0.39 and -0.34 with monthly resolution, and r = 0.67 and -0.60 with yearly resolution). Consistent with Nakamura and Kazmin (2003), the link between the subarctic front and ENSO seems small, with only a weak SST anomaly in the equatorial Pacific.

b. Definition of the KE index

The KE index (KEI) is based on the first PC of the latitude of the 14°C isotherm at 200 m between 142° and 160°E. The 200 m level maximizes data availability while remaining below the winter mixed layer, but it is above the strongest subsurface front, so that it may not fully represent the position of the surface jet. The 200 m temperature was objectively mapped for each 3 months from JFM 1979 to OND 2007 (e.g. JFM 1980, AMJ 1980 ... where months are denoted by their first letter) using the raw temperature profiles from the WOD2005 and its online updates. The latitude of the 14°C isotherm was selected at each longitude and time step. As the data are sparse and noisy because of the strong eddy activity in the KE (Qiu and Chen 2005), a triangular 5-point moving average was used to remove the variability less than a year, and data points from the first and last years, i.e. 1979 and 2007, are discarded. After removing a linear trend at each longitude, an EOF analysis was performed for the latitude of the 14°C isotherm with the smoothed seasonal data from JFM 1980 to OND 2006. The leading EOF represents uniform north-south shift of the KE and explains 70% of the total variance. One standard deviation change in the PC corresponds to a meridional shift of about

100 km. The normalized leading PC, after removal of the (small) mean seasonal cycle and a third-order trend, is used as KEI. The KEI is dominated by variability longer than a few years (Fig. 3a) and its auto-correlation function indicates weak oscillations at 12-14 yr period (not shown). A shorter version of the index was used in Joyce et al. (2009).

The SSH derived from satellite altimetry has been used to define a KE index starting in 1993 (e.g. Qiu and Chen 2005). The SSH-based KE index exhibits similar correlations with the SST index, but it is only moderately correlated (r = 0.52) with our 200 m temperature-based KE index. This could be due to our use of a relatively shallow level to define the KEI, which maximizes data availability while remaining below the winter mixed layer, yet may not be fully representative of the position of the subsurface jet.

The origin of the KE fluctuations was examined through the regression of wind stress curl and SLP anomalies onto the KEI (not shown). The SLP regression exhibits a northward shift and weakening of the Aleutian Low when SLP leads by 0-2 yr. The wind stress curl exhibits a band of negative values between 30°-45°N that almost extends across the whole basin, with a maximum near 160°W. The maximum correlation occurs when the wind stress curl leads the KEI by 2 yr. The correlation between the linear Rossby wave model SSH hindcast (averaged over 30°-40°N, 142-160°E) and the KEI is 0.60, which confirms that the KEI primarily reflects a baroclinic response to basin-scale wind stress curl forcing.

The KEI represents the subsurface KE front. The associated SST variability (Fig.6, top) shows a large signal in the KE region, as well as in the tropical Pacific where it resembles the second tropical Pacific EOF (see Fig.7 below). The simultaneous correlation with the (detrended) KE SST index in Fig. 1 is r = 0.39. However, the maximum correlation occurs when the SST index leads KEI by 2 seasons (r = 0.49). A similar lag is found for the

maximum anti-correlation between the PDO and the KEI, possibly in part because the SST responds faster to the atmospheric forcing than the KE.

c. Relation between the two indices

The KEI and the OEI (correspondingly smoothed) are practically uncorrelated (r = 0.16), even though they co-vary with the KE SST index and the PDO. Marginally significant correlations are found at lags of 2 to 3 yr, but they do not affect the analysis below, which is only based on short time lags.

4. Estimating the atmospheric response

a. Method

In most studies, the response to extratropical SST anomalies was derived from the relation between the atmosphere and prior SST anomalies, since the relation at no time lag or for the atmosphere leading is dominated by the oceanic response to the atmosphere. The method (Frankignoul et al. 1998) assumes that an atmospheric signal *X(t)* at a given location and time *t* can be decomposed into a short-time scale signal that characterizes the intrinsic variability of the atmosphere, say *n(t)*, and a linear function of an SST anomaly or any other slow variable such as a WBC index, say *T(t),*

$$X(t) = FT(t) + n(t) \qquad (1)$$

where *T(t)* has a much longer time scale than *n(t),* and *F* is the response or feedback. Multiplying (1) by $T(t-\tau)$ and taking ensemble average leads to

$$C_{XT}(\tau) = FC_{TT}(\tau) + C_{nT}(\tau) \qquad (2)$$

where $C_{XT}(\tau)$ denotes the lagged covariance between *X* and *T*, and a positive τ indicates that the atmosphere lags the ocean. For τ much larger than the intrinsic atmospheric persistence, $C_{nT}(\tau) = 0$, and *F* can be estimated by

$$F = \frac{C_{XT}(\tau)}{C_{TT}(\tau)} \tag{3}$$

Recent model studies suggest that the atmospheric response to extratropical SST anomalies takes a few months to fully develop, reflecting the time it takes for the transient eddy-mean flow interactions to transform the initial baroclinic response into a larger equivalent barotropic one (Ferreira and Frankignoul 2005, 2008; Deser et al. 2007). Such a delay would be consistent with the stronger covariance found in the observations when the atmosphere follows the SST anomalies by at least 2 months (Czaja and Frankignoul 2002; FS07). In this case, relation (1) should take a more complex form, but it can be coarsely approximated by replacing *T(t)* by *T(t-d)*, where *d* is a characteristic delay time. We use *d* = 2 months, consistent with Deser et al. (2007). Relation (3) then becomes for $\tau \geq d$

$$F = \frac{C_{XT}(\tau)}{C_{TT}(\tau - d)} \tag{4}$$

The multivariate generalization to vector fields is straightforward (Liu et al. 2008). In this paper, we only use univariate estimates, hence consider the OEI and the KEI separately. This is consistent with their negligible correlation and is also motivated by the different temporal resolution and slightly different time period. However, it should be kept in mind that the estimated atmospheric response may also be influenced by co-varying SST (or other) anomalies at different locations.

In the presence of ENSO teleconnections, there is an additional persistent atmospheric component and the decomposition (1) must be generalized into

$$X(t) = FT(t - d) + be(t) + n(t) \quad (5)$$

where b is a parameter, $e(t)$ is the ENSO time series, assuming a fast atmospheric response to the tropical SST. As shown by Frankignoul and Kestenare (2002) and in Appendix 1, F can still be estimated provided the ENSO influence is first removed from both X and T, and $e(t)$ and $n(t)$ are uncorrelated. Although the latter assumption holds on short time scales, it does not on long time scales because of the seasonal footprinting mechanism of Vimont et al. (2003), in which the tropical atmosphere is forced during spring and summer by SST anomalies generated by the NPO during the previous winter. Hence, our assumption that $e(t)$ and $n(t)$ are uncorrelated should be viewed with caution for the KE, since the KEI only resolves relatively long time scales for which the subtropical-tropical link may become effective.

In this paper, the ENSO signal is given by the first three PCs of monthly SST anomalies in the tropical Pacific between 12.5°N and 12.5°S. The first mode (61% of the variance) roughly corresponds to NINO3.4. The second (14% of the variance) represents the east-west SST contrast. The third mode (4% of the variance) has a narrow maximum along the equator. The associated SST anomalies (Fig. 7) are substantial in the North Pacific. Two PCs or indices are generally used to represent the different types of ENSO (e.g., Trenberth and Stepaniak 2001; Kao and Yu 2009) and the SST asymmetry between El Niño and La Niña (Hoerling et al. 1997; Straus and Shukla 2002). The third one was included as it plays a role at the end of the ENSO events (see Fig. 9 below). The results in section 5 are similar when only using the first two PCs, but the response to the OE fluctuations is slightly larger and more significant when adding the third one. Prior to the analysis, a cubic polynomial was removed from all variables by least squares fit, to reduce the influence of trends and ultralow-frequency changes. Similar results were obtained by removing a quadratic trend.

To take into account the asymmetry of the ENSO teleconnections, the ENSO signal was removed from the atmospheric fields and the WBC indices by multivariate regression, distinguishing between positive and negative values of the PCs, so that the regression is based on 6 time series which are only pair-wise uncorrelated. To take into account the seasonality of the ENSO teleconnections, the regression coefficients are seasonally varying. To get smoothly varying estimates, the multivariate regression for a particular calendar month also uses the preceding and the following month (for example, the regression for February is calculated from January, February, and March of each year). The analysis was also conducted without taking seasonality into account, with broadly similar results. Omitting the asymmetry in the ENSO removal has stronger effects, but did not substantially change the results. The seasonal KEI is too smoothed to resolve seasonal modulation, but for consistency the ENSO PCs were also smoothed when removing the ENSO influence from the KEI.

Statistical significance was estimated in two ways, with similar results. First, we tested the correlation between $X(t)$ and $T(t-\tau)$, taking into account the time series persistence (e.g., Bretherton et al. 1999). Statistical significance was then verified non-parametrically, using a block bootstrap approach (randomly permuting the atmospheric time series 500 times in blocks of 2 yr for the OEI and 3 yr for the KEI) (e.g., von Storch and Zwiers 1999). The non-parametric approach is used in the figures below. Since the Ekman pumping field is noisy, we use the 10% significance level, but similar results are found at the 5% level.

It should be stressed that the ENSO removal, as done in this study, is solely aimed at estimating the atmospheric response to extratropical boundary forcing. It does not separate the response of the WBCs to the extratropical atmospheric variability from that to ENSO teleconnections because the WBCs respond as integrators of the atmospheric forcing, thus

depending on their time history. Separation could only be attempted by using a specific model of the WBC response, as done for SST in Schneider and Cornuelle (2005).

b. ENSO teleconnections

The asymmetry in the atmospheric anomalies associated with the ENSO PCs varies with the time of year. A typical example is shown for Z250 in March by the regression maps in Fig. 8. If symmetric, the regressions for positive and negative values should be identical within sampling error. However, there is relative symmetry for PC1 but a strong asymmetry for PC2 and PC3, especially near the KOE. The signal, baroclinic in the tropics and equivalent barotropic elsewhere, typically reaches about 50 m in winter and 20 m in summer at 250 hPa for PC1, and somewhat less for PC2. It is shown below that the estimated North Pacific response at 250 hPa to typical WBC changes is 15 m for the KE and 35 m for the OE. Hence, the removed ENSO signal may be larger than the signal of interest, consistent with the larger efficiency of tropical boundary forcing compared to midlatitude one (e.g. Kushnir et al 2002). This stresses the importance of removing the ENSO teleconnections as carefully as possible.

The efficiency of the ENSO removal is illustrated for SST as it shows that the SST residual is negligible in the tropics where efficient boundary forcing could take place. The SST anomalies associated with the ENSO events can be described by composites. In the period of interest, the "year 0" El Niño events take place in 1982, 1987, 1997, 2002, 2004, and 2006, and La Niña events in 1988, 1998, 1999, and 2007. The difference between the El Niño composite and La Niña composite (based on the NCEP SST data) is shown for FMA of "year 1" in Fig. 9 (left), near the peak of the ENSO events. The SST signal linked to ENSO is dominated by the regressions on PC1, but is also affected by PC2 and, to a much lesser

extent, PC3, as shown by the comparison between the SST residual based on PC1 only (middle panel) and that based on all three PCs (bottom panel). ENSO filtering has often been based on the NINO 3.4 index (e.g., Liu et al. 2006, Qiu et al 2007), which roughly corresponds to ENSO PC1. Figure 9 shows that a single index does not suffice to remove the SST signal in the tropics, but that three indices do it reasonably well. This holds for the atmospheric ENSO teleconnections. Using the second and third tropical Pacific PCs in the regressions has also reduced the SST residual in the North Pacific. However, a substantial signal (recall that it is an average of, presumably, independent events) remains in the KE and OE region, due to intrinsic mid-latitude atmospheric forcing and WBC changes (that may in part be a lagged response to ENSO forcing).

The ENSO removal is illustrated for JAS(1), when the ENSO events are largely terminated (Fig. 9, right). The comparison between the residuals using 2 (middle) and 3 (bottom) PCs shows that the SST signal linked to the third ENSO PC has become large at tropical and extratropical latitudes. The largest contribution arises from the La Niña events.

5. Response of the atmosphere to OE and KE fluctuations

a. Influence of the OE shifts

As shown in Fig. 5, although the OEI is little affected by ENSO removal, it has become virtually uncorrelated with tropical SST. A significant influence of the OE variability onto the large-scale atmospheric circulation in the North Pacific sector is detected using (4) when the OEI leads by 2 to 6 months. The patterns are robust to ENSO removal, although the signal is slightly larger and more significant when the three ENSO PCs are used. Because of atmospheric persistence, lag 1 may also be strongly contaminated by the atmospheric forcing of the OE fluctuations.

As illustrated in Fig. 10, the atmospheric response is primarily an equivalent barotropic meridional dipole over the North Pacific, with a large low centered near the dateline at 55°N and an elongated mid-latitude high with two maxima. The pattern is similar to the wintertime NPO/WP patterns (c.f. Linkin and Nigam 2008), except for the high found south and slightly downstream of the OE front. However, the latter is not as strong when the atmospheric response is estimated for the cold season (see Fig. 12 below). The signal is most significant in the middle and upper troposphere (Z250 and Z500). It reaches at 250 hPa about 25 m for the southern lobe and 35 m for the northern one, 25% less at 500 hPa, and respectively 0.8 and 1.7 hPa for SLP. It is associated with significant hemispheric teleconnections, in particular significant highs above northeastern America and western Europe, as in the WP pattern (Fig. 11, top). Since the OEI is normalized, this represents the typical magnitude of the signal. However, the amplitude should be viewed with caution as it varies with the lag and the assumed 2-month response time. Assuming an instantaneous response ($d = 0$) would double the amplitude in Fig. 10 while using a longer delay would decrease it.

The Ekman pumping is noisy and more dependent on the lag, yet suggestive of a significant meridional dipole pattern in the central North Pacific, with Ekman suction along 55°N and Ekman pumping between 30°N and 45°N (Fig. 10, bottom). Typical fluctuations reach 5×10^{-7} m s^{-1}. The response to a northward shift of the OE should strengthen the East Kamchatka Peninsula Current. It should also decrease the Oyashio Current strength and shift the OE northward since the Ekman pumping is negative along the OE. The OE meridional shifts are largely forced by fluctuations in the Aleutian low and associated PNA pattern (section 3a). Although there is little resemblance between forcing and response patterns in the troposphere (compare Fig. 10 and Fig. 4), the Ekman pumping pattern that precedes the OEI

shift broadly resembles that which follows it, presumably because the Ekman pumping response consists of two components, one proportional to the Laplacian of SLP and another linked to the atmospheric boundary layer response to the SST front (Felix et al. 2004; Kelly et al. 2010; Kwon et al. 2010b). Since Ekman pumping plays the leading role in generating the OE shifts, the atmospheric response should act as a weak positive feedback.

A significant asymmetry in the atmospheric response was found when considering separately the northward and southward migration of the OE, although it should be considered with caution in view of the limited sample. As illustrated in Fig. 12, the signal at 250 hPa is slightly stronger and more significant for negative OEI (southward migration. A similar asymmetry is found for SLP, which is only 10 % significant for negative OEI (bottom panel), and for the Ekman pumping (not shown). A dependence on SST polarity is often found in sensitivity studies with atmospheric models (e.g. Kushnir and Lau 1992; Peng et al. 2002), reflecting the importance of the transient eddy-mean flow interactions that largely control the mid-latitude atmospheric response to SST forcing.

The seasonal variability of the response was investigated at 250 hPa by considering sets of three successive months per year for the atmosphere and the OEI. Due to the smaller sample, we did not differentiate between positive and negative OE shifts. The most robust signal appears in winter (NDJFM), mostly at lag 2 and 3, so that late summer to early fall values of the OEI should have some predictive values for the atmospheric circulation a few months later. As shown in Fig. 13, the winter atmospheric signal in NDJ as estimated from SST in ASO is slightly shifted northeastward, and its similarity with the winter NPO/WP pattern is more striking.

b. Influence of the KE meridional shifts

Contrarily to the OEI, the detrended KEI is substantially modified by ENSO removal, which decreases its standard deviation by 23 % (Fig. 14). A comparison with the KEI residual obtained by neglecting the asymmetry in the ENSO removal shows that there are significant differences with the asymmetric case, albeit smaller than with the original detrended index. Because of the smoothing, the seasonal effects are negligible. The strong effect of the ENSO removal is due to the second ENSO PC, which is highly anti-correlated (r = -0.54) with the KEI, consistent with Fig. 6 (top). Links between the KE and tropical Pacific SST, and its relation to the North Pacific Gyre Oscillation are examined by Di Lorenzo et al. (2008). Figure 6 (bottom) shows that the tropical SST associated with the KEI is removed by the multivariate regression, except for a small signal in the Indian Ocean and in the eastern Pacific.

To search for an atmospheric impact of the meridional shifts of the KE jet, we applied for consistency the triangular 5-point smoothing to the seasonal anomalies of the atmospheric fields. As a result, maps based on (4) are not independent at successive lags. Since lag 0 primarily reflects the oceanic response to the atmospheric forcing, we estimate the atmospheric response from a lag of 2 seasons (Fig. 15). The signal resembles that at lag 1, 3 and 4, while drastically differing from the patterns found when the atmosphere leads by 1 or 2 seasons. Hence, it appears to indeed represent an atmospheric response.

Figure 15 suggests a primarily equivalent barotropic response at mid and high latitudes, but with a high in the northwestern North Pacific that tilts westward with height, suggestive of baroclinic structure, and a much weaker low along the KOE region. In addition, the SLP signal shows a significant high in the subtropical western Pacific that might be indicative of a wave train coming from the tropics. The regression of the SST field onto the KEI after ENSO removal only shows a weak signal in the western Indian Ocean, but a

contamination by Indian Ocean SST forcing cannot be completely ruled out (Fig. 6 bottom). The upper tropospheric pattern is similar to the 500 hPa winter correlation map shown by Hirose et al. (2009) to follow the changes in the Tsushima Warm Current by one season. If a northward shift of the KE corresponds to an intensification of the Kuroshio transport (Qiu and Chen 2005) and the Tsushima Warm Current co-varies with the KE, the two signals are consistent. Hirose et al. (2009) suggested that the pattern resembled the WP teleconnection pattern, although the signal was shifted westward compared to traditional estimates (Linkin and Nigam 2008). This is also the case in Fig. 15. Since the mid-latitude lobe is much weaker than in the NPO/WP pattern and its hemispheric extension (Fig. 11, bottom) is very different, it seems questionable to call it WPO/WP-like. The Ekman pumping response to the KE shift (Fig. 15, bottom) shows a banded pattern in the central and western North Pacific (more significant at lag 1) with (positive) Ekman suction in the KOE region and (negative) Ekman pumping south of it. Also noteworthy is a broad region of positive Ekman pumping in the southeastern part of the domain, as found by Qiu et al (2007) in a regression on the KE SST box.

Since the KEI is based on seasonal means, the amplitude of the response was estimated by using $d=1$, thus assuming an atmospheric response delay of one season, rather than 2 months as before. This may lead to a slight underestimation of the response, but it is difficult to quantify because of the KEI smoothing. The tropospheric high in Fig. 15 reaches 15 m at 250 hPa and 0.6 hPa for SLP, so that the response to the KE shifts is at least twice weaker than in the OE case. This is broadly consistent with the smaller SST signature of the KEI (compare Fig. 4 and 6), leading thru the negative heat flux feedback to smaller diabatic heating of the atmosphere.

6. Summary and discussion

After removing the ENSO teleconnections in a seasonally varying, asymmetric way, the meridional shifts of the OE and the KE were shown to have a significant influence on the large-scale tropospheric circulation. The response patterns and their statistical significance are robust to detrending and to the particular way the ENSO signal is removed, in particular in the OE case, as long as at least two indices are used to characterize ENSO. On the other hand, the estimated amplitudes are sensitive to the assumed 2-month delay in the atmospheric response.

A strong equivalent barotropic atmospheric signal lags the meridional shifts of the OE front. The response resembles an NPO/WP pattern in a positive phase for a northward shift and in a negative phase for a southward shift, with significant teleconnections over northeastern North America and Western Europe. It is more significant when the front is displaced southward, although some caution is advised on the significance of the nonlinearity, given how short the data records are. When the data are seasonally stratified, the signal can only be detected in winter (NDJFM), and it is even more NPO/WP-like. Linkin and Nigam (2008) have shown that a positive NPO phase is associated with a meridionally tighter and eastward-extended storm track. Hence, the response to the meridional shifts of the OE front may be linked to the anchoring effect of oceanic frontal zones on storm development (Nakamura et al. 2004). The wind stress curl pattern that primarily forces the meridional OE shifts and that which responds to them show some similarity, suggesting that a weak positive feedback may reinforce the variability of the North Pacific subpolar gyre. The response to typical OE shifts seems to be large, typically reaching about 35 m at 250 hPa and 25% less at 500 hPa. As the SST anomaly associated with the OE shifts is about 0.5K, our estimate of the atmospheric sensitivity is larger than that suggested by AGCM response studies (e.g., Kushnir et al. 2002; Peng et al. 2003), which ranges between 20 and 40 mK^{-1} at 500 hPa. However,

none of the AGCMs had enough spatial resolution to represent the sharp SST front associated with the OE, which is crucial to favor the storm track development.

A significant tropospheric response was also found for the KE shifts, which were derived with less temporal resolution (due to data limitation) from the temperature at 200 m depth along the KE mean axis. The response to a northward shift is an equivalent barotropic high centered in the northwestern North Pacific, with a much weaker low in the KOE region. It closely resembles the winter signal found by Hirose et al. (2008) when the transport of the Tsushima Warm Current was larger in the preceding fall, which would be consistent if a northward shift of the KE was associated with a strengthening of the Kuroshio, as suggested by Qiu and Chen (2005), and the Tsushima Warm Current was fluctuating in phase with the KE. The response to the KE shifts is displaced westward compared to the traditional NPO/WP pattern and its southern lobe is too weak to be referred to as NPO/WP-like, as in Hirose et al. (2008). Moreover, its hemispheric extension is different, with a low over northern Europe. Note that the SST warming associated with KE shifts differs from, and extends further eastward than, that associated with the OE, resulting in a different influence on the atmosphere. Although the Ekman pumping response to the KE shifts differs in the western half of the basin from the response to the SST anomalies in the KE box discussed by Qiu et al. (2007), it may still act as a (delayed) negative feedback as it should reduce the KE strength and shift it southward. The typical response amplitude is smaller than for the OE shifts, reaching about 15 m at 250 hPa, but the SST associated with the KE shift is smaller.

A summer tropospheric signal was found by FS07 to be significantly linked to previous basin-wide SST anomalies with maximum amplitude in the KE region (see also Kwon et al. 2010a), and they speculated that it was related to the variability of the KE. Our KEI is too smoothed to investigate seasonal influence, but the response to the KE shifts

estimated here is very different. In addition, no significant influence of the OE shifts could be detected in summer. Hence, the summer signal in FS07 is unlikely to be driven by meridional WBC shifts, presumably because the SST fronts are weaker and radiative processes more influential during summer.

A number of issues require further investigation. The atmospheric fields were taken from the NCAR-NCEP reanalysis, which uses the coarse resolution SST. The atmosphere could thus not respond to sharp SST fronts. Although it is hoped that the atmospheric observations assimilated in the model could nudge the large-scale response to the one driven by the small frontal shifts considered here, a higher resolution reanalysis should be used. Our KEI is only moderately correlated with the KE index derived from satellite altimeter data. This difference may be linked to our use of a relatively shallow level (200 m) to define the KE, but it needs to be understood. Our analysis is based on univariate regression, consistent with the OEI and the KEI being virtually uncorrelated, but their influence on the atmosphere, which should primarily arise from local changes in SST and surface heat exchanges, cannot not be distinguished from that of the basin-scale SST anomalies that co-vary with the WBC shifts. We have assumed that the atmospheric ENSO teleconnections are in phase with the ENSO forcing, even though they take approximately 2-6 weeks to be established (Liu and Alexander 2007). Although our use of three ENSO PCs includes some lags (e.g. PC 2 tends to lead PC 1 by ~8 months) and the PCs are rather persistent, this is not strictly valid, nor is our assumption that the ENSO indices are uncorrelated with the intrinsic mid-latitude atmospheric variability. Also, the KEI after ENSO removal is still associated with a small tropical SST signal in the Indian Ocean and in the eastern equatorial Pacific, so that it cannot be excluded that the estimated response to the KE shifts is slightly contaminated. A more sophisticated multivariate procedure that simultaneously considers all the different boundary forcing should

better single out the direct influence of the WBC shifts. Finally, the amplitude (but not the pattern nor the significance) of the estimated response depends on an assumed 2 month-delay in the atmospheric response. This is an oversimplification based on AGCM response studies to North Atlantic SST anomalies. The transient response to North Pacific frontal shifts should be investigated with atmospheric models with sufficiently high resolution, and its dynamics elucidated.

Appendix 1. Removing ENSO

To estimate F from (5), let us define

$$\hat{X}(t) = X(t) - \frac{C_{Xe}}{C_{ee}} e(t) \tag{A1}$$

$$\hat{T}(t) = T(t) - \frac{C_{Te}(d)}{C_{ee}} e(t+d) \tag{A2}$$

where the lag of the covariance is omitted when it is zero. Replacing X by (5) and using (A2) yields

$$\hat{X}(t) = F\hat{T}(t-d) + \frac{FC_{Te}(d) + bC_{ee} - C_{Xe}}{C_{ee}} e(t) + n(t) \tag{A3}$$

Since n and e are uncorrelated ($C_{ne} = 0$), one has from (5)

$$C_{Xe} = FC_{Te}(d) + bC_{ee} \tag{A4}$$

Replacing in (A4) yields

$$\hat{X}(t) = F\hat{T}(t-d) + n(t), \tag{A5}$$

F can now be estimated by (4). The generalization to several ENSO time series is straightforward.

Acknowledgments

The NCAR/NCEP Reanalysis data was provided through the NOAA Climate Center (http://www.cdc.noaa.gov/). Discussion with B. Qiu and N. Schneider are acknowledged. This work was supported in part by the Institut universitaire de France (CF), the WHOI Heyman fellowship and the NASA grant with award # NNX09AF35G (Y-OK), and grants through NOAA's Climate Variability and Predictability Program (MAA).

References

Alexander, M. A., I. Bladé, M. Newman, J. R. Lanzante, N.-C. Lau, and J. D. Scott, 2002: The atmospheric bridge: the influence of ENSO teleconnections on air-sea interaction over the global oceans. *J. Climate*, **15,** 2205-2231.

Celallos, L.I., E. Di Lorenzo, C.D. Hoyos, N. Schneider, and B. Taguchi, 2009: North Pacific Gyre Oscillation synchronizes climate fluctuations in the eastern and western boundary systems. *J. Climate*, 22, 5163-5174.

Czaja, A. and C. Frankignoul, 1999: Influence of the North Atlantic SST on the atmospheric circulation, *Geophys. Res. Letters*, 26, 2969-2972.

Czaja, A. and C. Frankignoul, 2002: Observed impact of Atlantic SST anomalies on the North Atlantic oscillation. *J. Climate*, 15, 606-623.

Deser, C., R. Thomas, and S. Peng, 2007: The transient atmospheric circulation response to North Atlantic SST and sea ice anomalies. *J. Climate*, 20, 4751-4767.

Di Lorenzo, E., and Coauthors, 2008: North Pacific Gyre Oscillation links ocean climate and ecosystem change. *Geophys. Res. Lett.*, **35,** L08607, doi :10.1029/2007GL03283.

Feliks Y., M. Ghil, and E. Simonnet, 1994 : Low-frequency variability in the midlatitude atmosphere induced by an oceanic thermal front. J. Atmos. Sci., 61, 961-981.

Ferreira, D. and C. Frankignoul, 2005: The transient atmospheric response to midlatitude SST anomalies. *J. Climate*, **18**, 1049-1067.

Ferreira D. and C. Frankignoul, 2008: Transient atmospheric response to interactive SST anomalies. *J. Climate*, 21, 576-583.

Frankignoul, C., A. Czaja, and B. L'Heveder, 1998: Air-sea feedback in the North Atlantic and surface boundary conditions for ocean models. *J. Clim*ate, **11**, 2310-2324

Frankignoul, C., G. de Coëtlogon, T.M. Joyce and S. Dong, 2001 : Gulf Stream variability and ocean atmosphere interactions. *J. Phys. Oceanogr.*, 31, 3516-3529.

Frankignoul, C. and E. Kestenare, 2002: The surface heat flux feedback. Part I: estimates from observations in the Atlantic and the North Pacific. *Clim. Dyn.* **19**, 633-647.

Frankignoul, C., and N. Sennéchael, 2007: Observed influence of North Pacific SST anomalies on the atmospheric circulation. *J. Climate*, 20, 592-606.

Hirose, N., K. Nishimura, and M. Yamamoto, 2009: Observational evidence of a warm ocean current preceding a winter teleconnection pattern in the northwestern Pacific. *Geophys. Res. Letters*, 36, L09705, doi:10.1029/2009GL037448.

Hoerling, M.P., A. Kumar, and M.Zhong, 1997: El Niño, La Niña, and the nonlinearity of their teleconnections. *J. Climate*, 10, 1769-1786.

Isoguchi, O., H. Kawamura, and T. Kono, 1997: A study of wind-griven circulation in the subarctic North Pacific using TOPEX/POSEIDON altimeter data. *J. Geophys. Res.*, 102, 12457-12468.

Johnson, D.R., T.P. Boyer, H.E. Garcia, R.A. Locarnini, A.V. Mishonov, M.T. Pitcher, O.K. Baranova, J.I. Antonov, and I.V. Smolyar, 2006: *World Ocean Database 2005 Documentation*. Ed. S. Levitus. NODC Internal Report 18, U.S. Government Printing Office, Washington, D.C., 163 pp.

Joyce, T.M., Y.-O. Kwon, and L. Yu, 2009: On the Relationship between Synoptic Wintertime Atmospheric Variability and Path Shifts in the Gulf Stream and the Kuroshio Extension. *J. Climate*, 22, 3177-3192.

Kao, H.-S. and J.-Y. Yu, 2009: Contrasting eastern–Pacific and central–Pacific types of ENSO. *J. Climate*, 22, 615-632.

Kelly, K.A., R.J. Small, R.M. Samelson, B. Qiu, T.M. Joyce, M. Cronin, and Y.-O. Kwon, 2010: Western Boundary Currents and Frontal Air-Sea Interaction: Gulf Stream and Kuroshio Extension. *J. Climate*, in press.

Kistler, R. and Coauthors, 2001: The NCEP-NCAR 50-year reanalysis: Monthly means CD-ROM and documentation. *Bull. Amer. Meteor. Soc.*, 82, 247-267.

Kushnir Y. and L.C. Lau, 1992 : The general circulation model response to a North Pacific SST anomaly: dependence on timescale and pattern polarity. *J. Climate*, 5, 271–283.

Kushnir, Y., W.A. Robinson, I. Bladé, N.M.J. Hall, S. Peng, and R. Sutton, 2002: Atmospheric GCM response to extratropical SST anomalies: synthesis and evaluation. *J. Climate*, **15**, 2233-2256.

Kwon, Y.-O. and C. Deser, 2007: North Pacific decadal variability in the Community Climate System model version 2. *J. Climate*, 20, 2416-2433.

Kwon, Y.-O., M.A. Alexander, N.A. Bond, C. Frankignoul, H. Nakamura, B. Qiu, and LA Thompson, 2010a: Role of Gulf Stream, Kuroshio-Oyashio and their extensions in large-scale atmosphere-ocean interaction : A review. *J. Climate*, in press.

Kwon, Y.-O., C. Deser, and C. Cassou, 2010b: Coupled atmosphere – mixed layer ocean response to ocean heat flux convergence along the Kuroshio Current Extension. *Climate Dyn.*, DOI 10.1007/s00382-010-0764-8.

Latif, M., and T. P. Barnett, 1994: Causes of decadal climate variability over the North Pacific and North America. *Science*, **266**, 634-637.

Liu, Z. and M. Alexander, 2007: Atmospheric bridge, oceanic tunnel, and global climatic teleconnections. *Rev. Geophys.,* 45, RG 2005.

Linkin, M.E.S. and Nigam, 2008: The North Pacific Oscillation–West Pacific Teleconnection Pattern: Mature-Phase Structure and Winter Impacts. *J. Climate*, 21, 1979–1997.

Liu, Q., N. Wen and Z. Liu, 2006: An observational study of the impact of the North Pacific SST on the atmosphere. *Geophys. Res. Letters*, 33, L18611, doi:10.1029/2006GL026082.

Liu, Z. and M.Alexander, 2007: Atmosqpheric bridge, oceanic tunnel, and global climatic teleconnections. *Rev. Geophys.*, 45, RG2005.

Liu, Z., N. Wen and Y. Liu, 2008: On the assessment of non-local climate feedback: I: the generalized Equilibrium Feedback Analysis. *J. Climate*, **21**, 134-148.

Mantua, N. J., S. R. Hare, Y. Zhang, J. M. Wallace, and R. Francis, 1997: A Pacific interdecadal climate oscillation with impacts on salmon production, *Bull. Amer. Meteor. Soc.*, **78**, 1069-1079.

Minobe, S., A. Kuwano-Yoshida, N. Komori, S. Xie, and R. J. Small, 2008: Influence of the Gulf Stream on the troposphere. Nature, 452, 206–209.

Nakamura, H., G. Lin, and T. Yamagata, 1997: Decadal climate variability in the North Pacific during the recent decades. *Bull. Am. Meteorol. Soc.*, 78, 2215-2225.

Nakamura, H. and A. Kazmin, 2003: Decadal changes in the North Pacific oceanic frontal zones as revealed in ship and satellite observations. *J. Geophys. Res.* 108, 3078, doi: 10.1029/1999JC000085.

Nonaka, M., H. Nakamura, Y. Tanimoto, T. Kagimoto, and H. Sasaki, 2006: Decadal Variability in the Kuroshio–Oyashio Extension Simulated in an Eddy-Resolving OGCM. *J. Climate*, 19, 1970–1989.

Nonaka, M., H. Nakamura, Y. Tanimoto, T. Kagimoto, and H. Sasaki, 2008: Interannual-to-decadal variability in the Oyashio Current and its influence on temperature in the subarctic frontal zone: An eddy-resolving OGCM simulation. *J. Climate,* **21**, 6283-6303.

Peng, S, W.A. Robinson and S. Li, 2003: Mechanisms for the NAO responses to the North Atlantic SST tripole. *J. Climate,* 16, 1987–2004

Pierce, D. W., T. P. Barnett, N. Schneider, R. Saravanan, D. Dommenget, and M. Latif, 2001: The role of ocean dynamics in producing decadal climate variability in the North Pacific. *Climate Dyn.,* **18,** 51–70.

Qiu, B., 2000: Interannual variability of the Kuroshio Extension and its impact on the wintertime SST field. *J. Phys. Oceanogr.,* **30,** 1486–1502.

Qiu, B., 2002: Large-scale variability in the midlatitude subtropical and subpolar North Pacific Ocean: Observations and causes. *J. Phys. Oceanogr.*, **32**, 353–375.

Qiu, B., 2003: Kuroshio Extension variability and forcing of the Pacific decadal oscillations: Responses and potential feedback. *J. Phys. Oceanogr.,* **33,** 2465–2482.

Qiu, B., and S. Chen, 2005: Variability of the Kuroshio Extension jet, recirculation gyre and mesoscale eddies on decadal timescales. *J. Phys. Oceanogr.*, **35**, 2090-2103.

Qiu, B., N. Schneider, and S. Chen, 2007: Coupled variability in the North Pacific: Observationally constrained idealized model. *J. Climate,* **20**, 3602–3620

Reynolds, R. W., T. M. Smith, C. Liu, D. B. Chelton, K. S. Casey and M. G. Schlax, 2007: Daily High-resolution Blended Analyses for sea surface temperature. *J. Climate*, 20, 5473-5496.

Rodwell, M.J. and C.K. Folland, 2002: Atlantic air-sea interaction and seasonal predictability. *Q. J. Roy. Met. Soc.*, 128, 1413-1443.

Schneider, N., A. J. Miller, and D. W. Pierce, 2002: Anatomy of North Pacific decadal variability. *J. Climate,* **15,** 586–605.

Schneider, N., and B. D. Cornuelle, 2005: The forcing of the Pacific decadal oscillation. *J. Climate,* **18,** 4355–4373.

Small, R. J., S. deSzoeke, S. P. Xie, L. O'Neill, H. Seo, Q. Song, P. Cornillon, M. Spall, and S. Minobe, 2008: Air–sea interaction over ocean fronts and eddies. *Dyn. Atmos. Oceans,* 45, 274-319.

Straus, D.M. and J. Shukla, 2002: Does ENSO force the PNA? *J. Climate*, **15**, 2340-2358.

Taguchi, B., S.-P. Xie, H. Mitsudera, and A. Kubokawa, 2005: Response of the Kuroshio Extension to Rossby waves associated with the 1970s climate regime shift in a high-resolution ocean model , *J. Climate*, **18**, 2979–2995.

Taguchi, B., H. Nakamura, M. Nonaka, and S.-P. Xie, 2009: Influence of the Kuroshio/Oyashio Extensions on the atmosphere simulated in a regional atmospheric model for the 2003/4 cold season. *J. Climate,* 22, 6536-6560.

Trenberth, K.E. and D.P. Stepaniak, 2001: Indices of El Niño evolution. *J. Climate*, 14, 1697-1701.

Vimont, D.J., J.M. Wallace, and D.S. Battisti, 2003: The seasonal footprinting mechanism in the Pacific: Implications for ENSO. *J. Climate*, 16, 2668-2675.

Vivier, F., K. A. Kelly, and L. Thompson, 2002: Heat budget in the Kuroshio Extension region: 1993–99. *J. Phys. Oceanogr.,* **32,** 3436–3454.

Von Storch, H. and F.W. Zwiers, 1999: *Statistical Analysis in Climate Research*. Cambridge University Press, 342 pp.

Wallace, J.M., and D.S. Grutzler, 1981: Teleconnections in the Geopotential Height Field during the Northern Hemisphere Winter, *Mon. Wea. Rev.*, 109, 784-812

Figure legends

Figure 1. (a) Mean SST (contour interval 1 °C) and standard deviation of monthly SST anomalies for 1982-2008, based on the NOAA OI 1/4° data. The black line defines the KE box. (b) Time series of the averaged SST anomalies in the KE box (shading) and of the PDO (black line).

Figure 2. Top: Hovmoller diagram of the latitude of maximum meridional SST gradient. Bottom: Mean position of the maximum meridional SST gradient (thin line) and its typical northerly position (thick line) as estimated from the first EOF and a unit value of the corresponding normalized PC.

Figure 3. Time series of (a) the KE index and (b) the OE index.

Fig.4 Regression of SLP and Ekman pumping on the OEI when the atmosphere leads by 1 month. White contours are for negative values and grey contours for positive ones. The black contour indicates 10% significance.

Figure 5. Regression of the SST anomalies onto the OEI, after removal of a cubic trend (top) and after also removing the ENSO signal (bottom). White contours are for negative values and grey contours for positive ones. The black contour indicates 10% significance.

Figure 6. Regression of the SST anomalies onto the KE, after removal of a cubic trend (top) and after also removing the ENSO signal (bottom). White contours are for negative values and grey contours for positive ones. The black contour indicates 10% significance.

Figure 7 Regression of the monthly SST anomalies (in K) onto the first (top), second (middle) and third (bottom) normalized PC of the (detrended) tropical Pacific SST anomalies. White contours are for positive values and grey contours for negative ones.

Figure 8 Regression of the geopotential height anomalies at 250 hPa (in m) onto positive (left) and negative (right) values of, from top to bottom, ENSO PC1, PC2, and PC3 in March, after removing a cubic trend. White contours are for negative values and grey contours for positive ones.

Figure 9 Difference between El Niño and La Niña composites (top), SST residuals when using ENSO PC1 (middle left) or ENSO PC1 and PC2 (middle right), and when using all three PCs (bottom) for FMA(1) (left) and JAS(1) (right). White contours are for negative values and grey contours for positive ones.

Figure 10. Estimated response in geopotential height at 250 hPa (top), SLP (middle), and Ekman pumping (bottom) to a unit value of the OEI (typical northward displacement), assuming $d = 2$ months, based on lag 3 ($\tau = 3$ months). White contours are for negative values and grey contours for positive ones. The dark contours indicate 10% significance.

Figure 11. Hemispheric response at 250 hPa to a unit value of the OEI (top) and the KEI (bottom). White contours are for negative values and grey contours for positive ones. The dark contours indicate 10% significance.

Figure 12. As in Fig.10 but for positive and negative values of the OEI at 250 hPa (top and middle panels, respectively) and negative values of OEI at SLP (bottom panel). White contours are for negative values and grey contours for positive ones. The black line indicates 10% significance.

Figure 13. Time series of the OEI in ASO after cubic detrending and ENSO removal (top) and estimated response of the geopotential height at 250 hPa in NDJ to a unit value of the OEI, assuming $d = 2$ months (bottom). White contours are for negative values and grey contours for positive ones. The dark line indicates 10% significance.

Figure 14. Time series of the normalized KEI after cubic detrending (thick grey line), and after also removing the ENSO signal linearly (grey line) or asymmetrically with seasonal dependence (thin black line). It is the latter curve that is used, after normalization, in the analysis to obtain the atmospheric response.

Figure 15. Estimated response to a unit value of the KEI, based on a lag of 2 seasons ($\tau = 2$), assuming an atmospheric response time of 1 season ($d = 1$). White contours are for negative values and grey contours for positive ones. The thick continuous line indicates the 10% significance level.

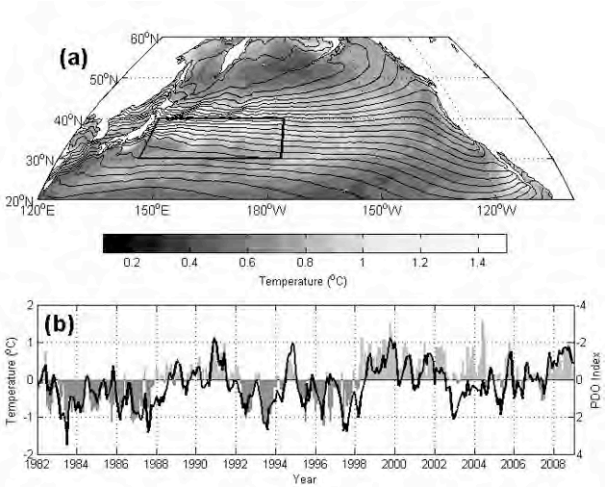

Figure 1. (a) Mean SST (contour interval 1 °C) and standard deviation of monthly SST anomalies for 1982-2008, based on the NOAA OI 1/4° data. The black line defines the KE box. (b) Time series of the averaged SST anomalies in the KE box (shading) and of the PDO (black line).

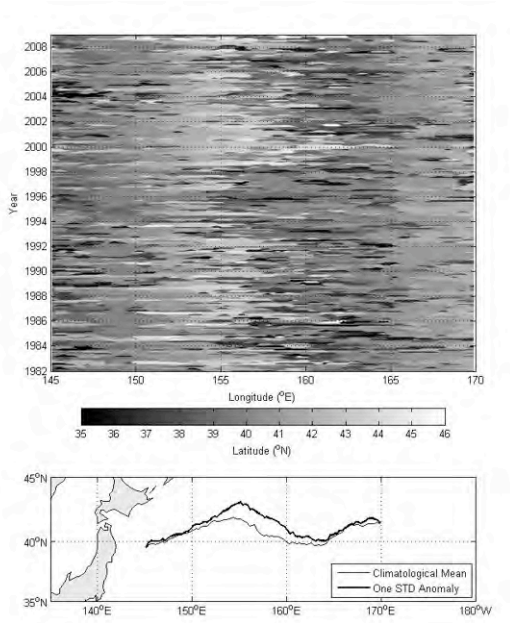

Figure 2. Top: Hovmoller diagram of the latitude of maximum meridional SST gradient. Bottom: Mean position of the maximum meridional SST gradient (thin line) and its typical northerly position (thick line) as estimated from the first EOF and a unit value of the corresponding normalized PC.

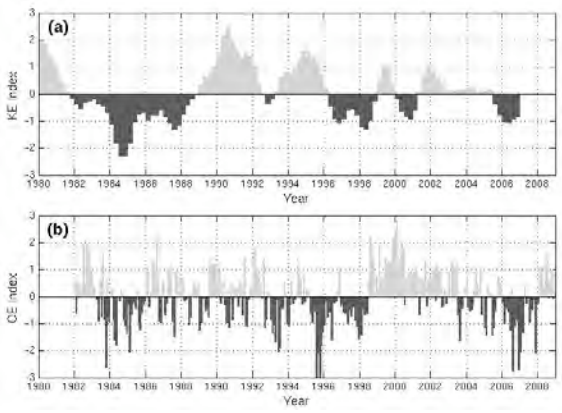

Figure 3. Time series of (a) the KE index and (b) the OE index.

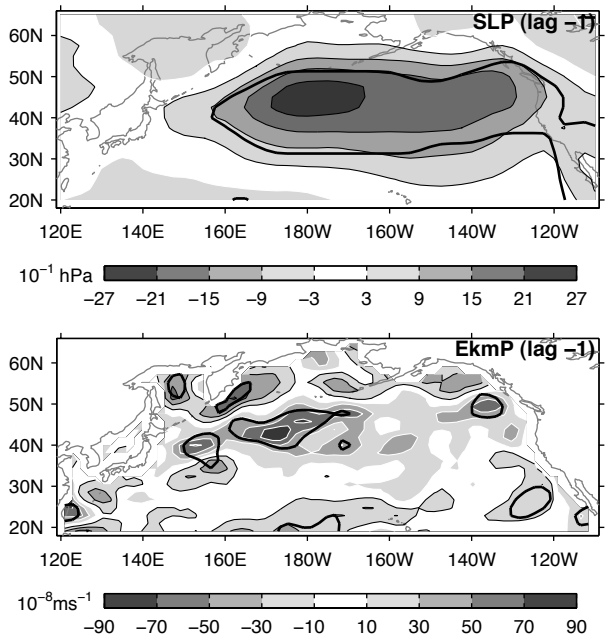

Figure 4. Regression of SLP and Ekman pumping on the OEI when the atmosphere leads by 1 month. White contours are for negative values and grey contours for positive ones. The black contour indicates 10% significance.

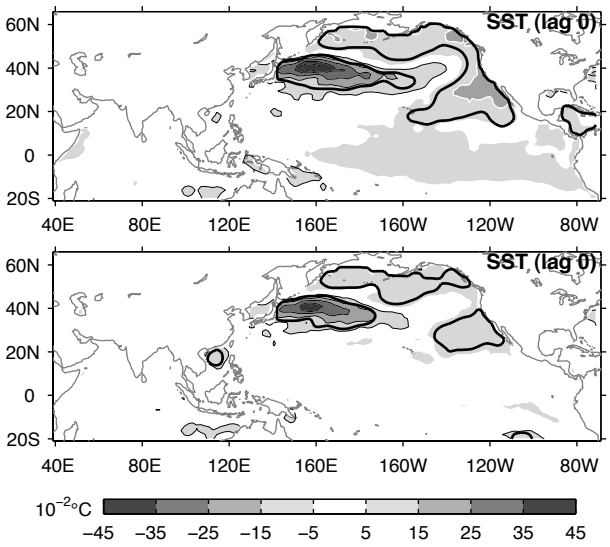

Figure 5. Regression of the SST anomalies onto the OEI, after removal of a cubic trend (top) and after also removing the ENSO signal (bottom). White contours are for negative values and grey contours for positive ones. The black contour indicates 10% significance.

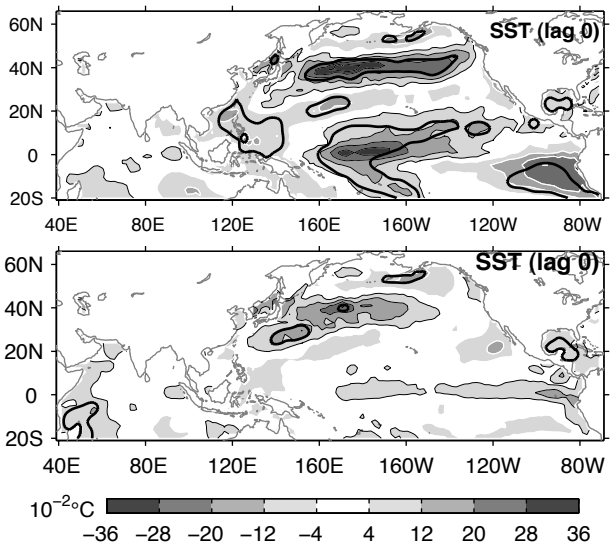

Figure 6. Regression of the SST anomalies onto the KE, after removal of a cubic trend (top) and after also removing the ENSO signal (bottom). White contours are for negative values and grey contours for positive ones. The black contour indicates 10% significance.

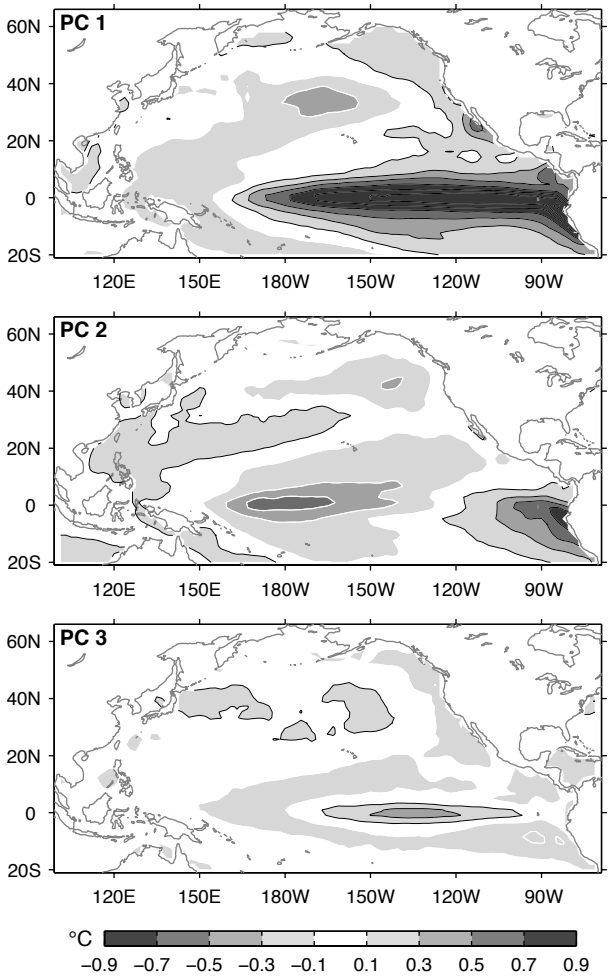

Figure 7 Regression of the monthly SST anomalies (in K) onto the first (top), second (middle) and third (bottom) normalized PC of the (detrended) tropical Pacific SST anomalies. White contours are for negative values and grey contours for positive ones.

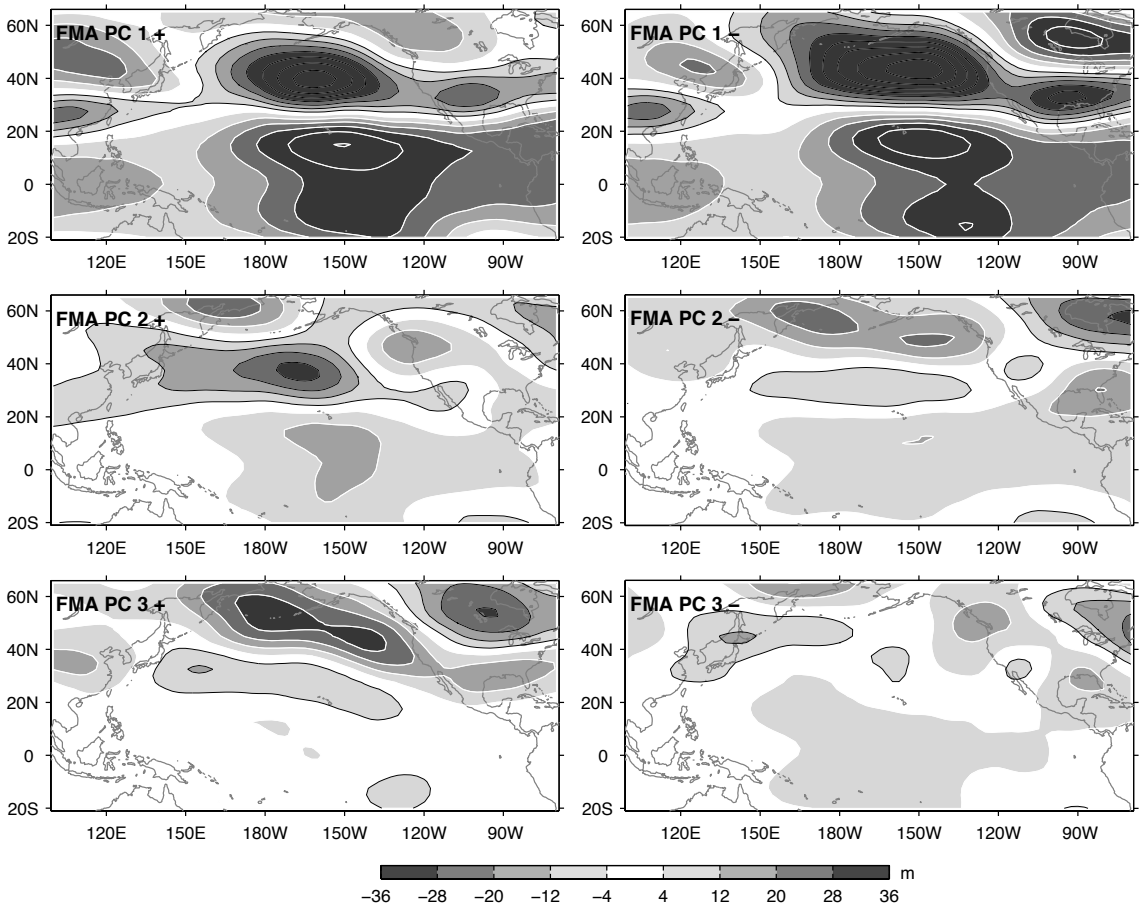

Figure 8 Regression of the geopotential height anomalies at 250 hPa (in m) onto positive (left) and negative (right) values of, from top to bottom, ENSO PC1, PC2, and PC3 in March, after removing a cubic trend. White contours are for negative values and grey contours for positive ones.

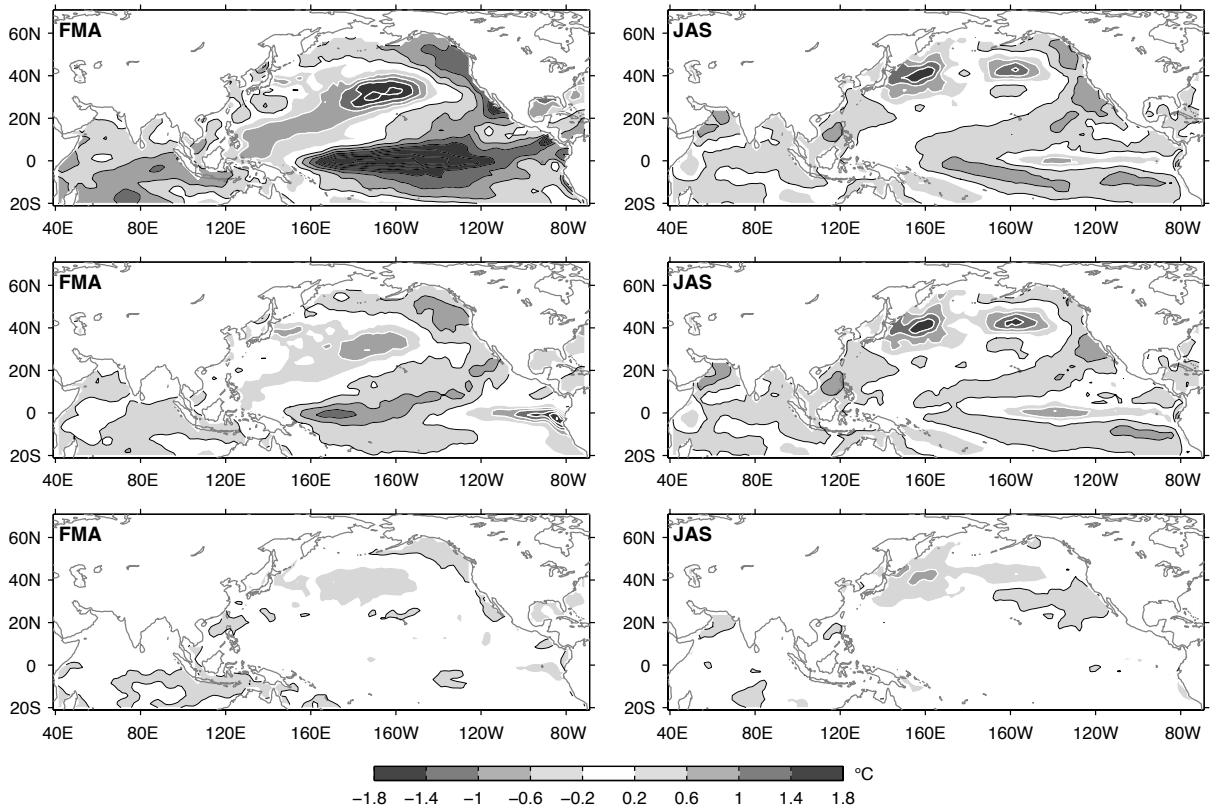

Figure 9 Difference between El Niño and La Niña composites (top), SST residuals when using ENSO PC1 (middle left) or ENSO PC1 and PC2 (middle right), and when using all three PCs (bottom) for FMA(1) (left) and JAS(1) (right). White contours are for negative values and grey contours for positive ones.

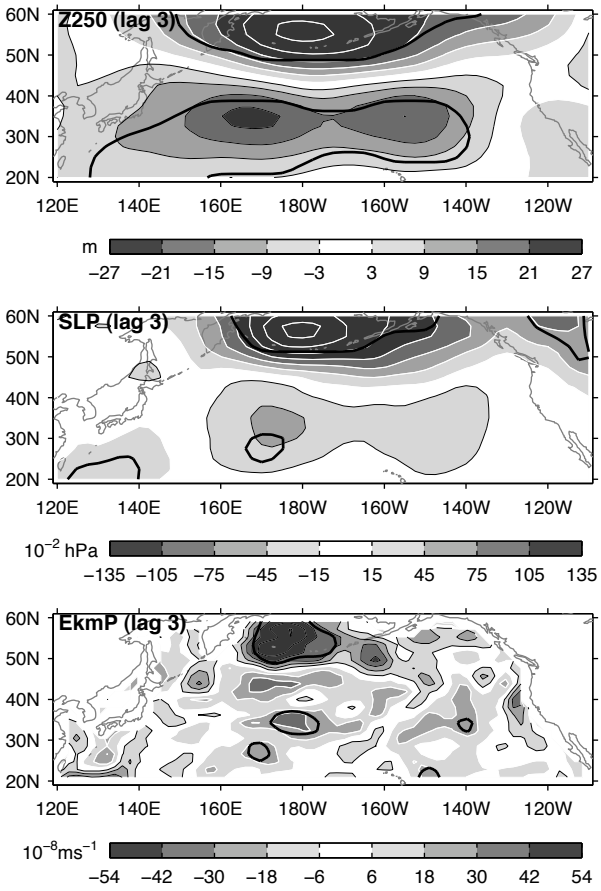

Figure 10. Estimated response in geopotential height at 250 hPa (top), SLP (middle), and Ekman pumping (bottom) to a unit value of the OEI (typical northward displacement), assuming $d = 2$ months, based on lag 3 ($\tau = 3$ months). White contours are for negative values and grey contours for positive ones. The dark contours indicate 10% significance.

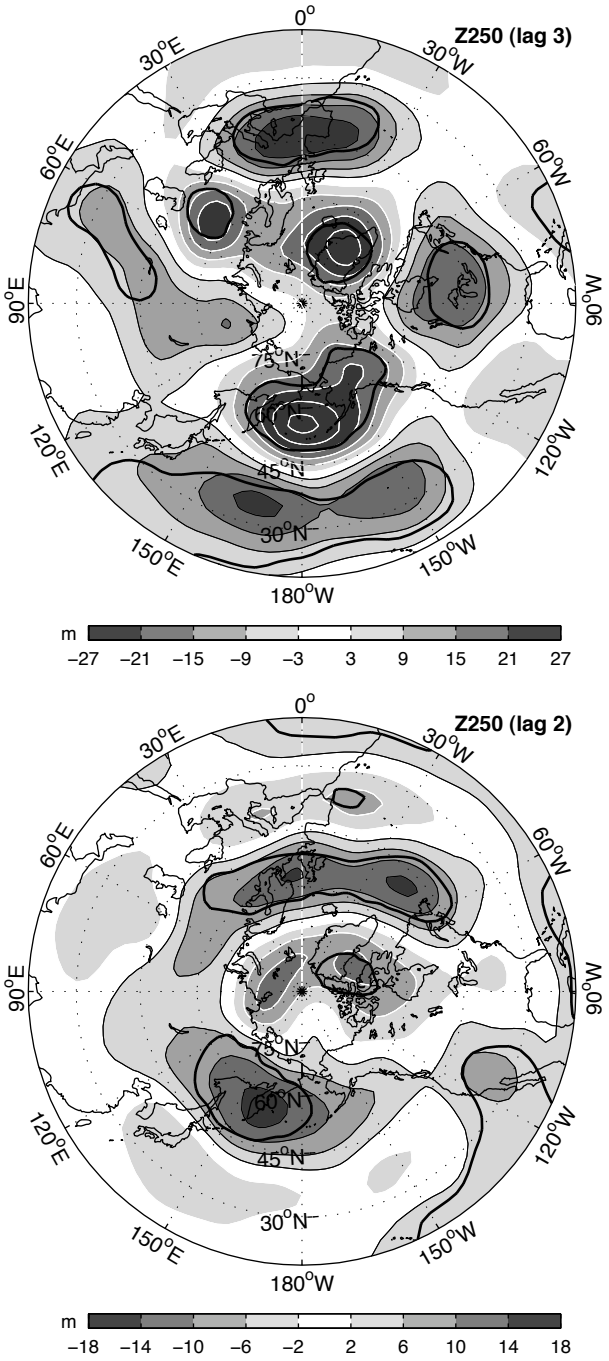

Figure 11. Hemispheric response at 250 hPa to a unit value of the OEI (top) and the KEI (bottom). White contours are for negative values and grey contours for positive ones. The dark contours indicate 10% significance.

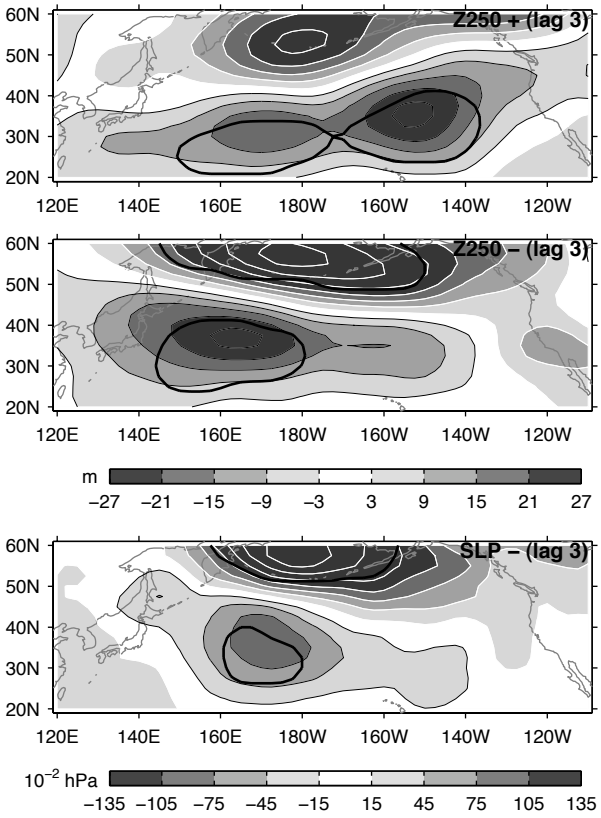

Figure 12. As in Fig.10 but for positive and negative values of the OEI at 250 hPa (top and middle panels, respectively) and negative values of OEI at SLP (bottom panel). White contours are for negative values and grey contours for positive ones. The black line indicates 10% significance.

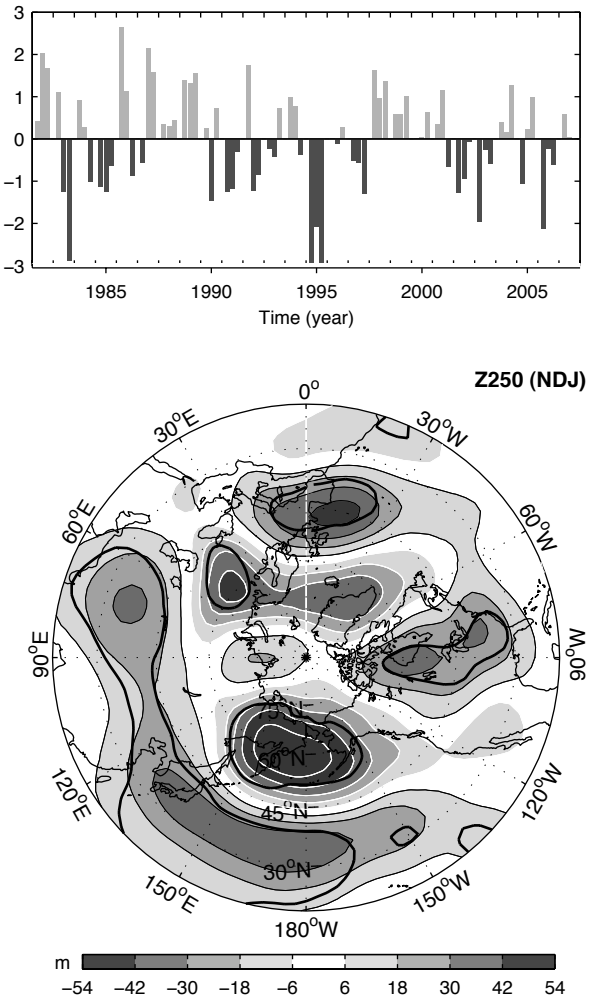

Figure 13. Time series of the OEI in ASO after cubic detrending and ENSO removal (top) and estimated response of the geopotential height at 250 hPa in NDJ to a unit value of the OEI, assuming d = 2 months (bottom). White contours are for negative values and grey contours for positive ones. The dark line indicates 10% significance.

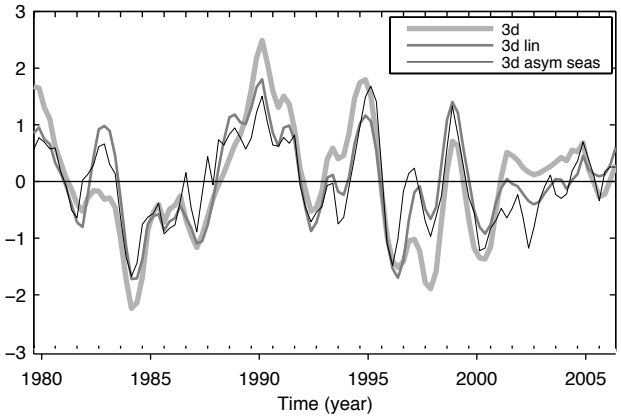

Figure 14. Time series of the normalized KEI after cubic detrending (thick grey line), and after also removing the ENSO signal linearly (grey line) or asymmetrically with seasonal dependence (thin black line). It is the latter curve that is used, after normalization, in the analysis to obtain the atmospheric response.

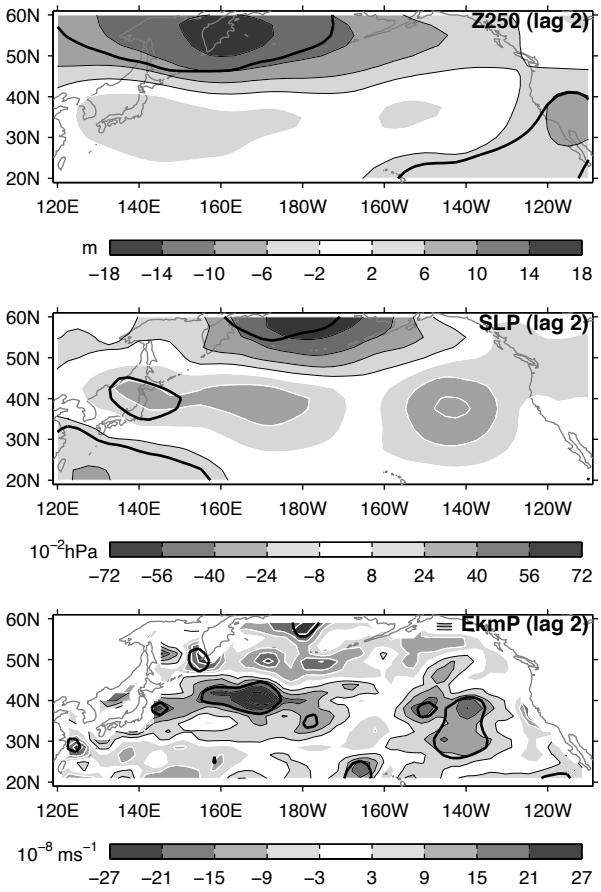

Figure 15. Estimated response to a unit value of the KEI, based on a lag of 2 seasons ($\tau = 2$), assuming an atmospheric response time of 1 season ($d = 1$). White contours are for negative values and grey contours for positive ones. The thick continuous line indicates the 10% significance level.